Revista Mexicana de Astronomía y Astrofísica, 61, 211-223, (2025)

OPEN ACCESS https://doi.org/10.22201/ia.01851101p.2025.61.03.09

Theory of Functional Connections Applied to the Temporary Gravitational Capture Problem

G. Afonso Siqueli[1], **A. K. de Almeida Junior**[1] **and A. F. B. A. Prado**[1]

[1]*Engineering and Space Technologies / Post Graduate division, National Institute of Space Research, Brazil.*

Keywords: *TFC, Theory of Functional Connections, Temporary Gravitational Capture*

Abstract

This paper presents applications of the Theory of Functional Connections (TFC) for solving problems in celestial mechanics, with a focus on temporary gravitational capture. The univariate TFC framework is employed to solve second-order differential equations. The mathematical formulation for the solution of the two-body problem and the circular restricted three-body problem (CR3BP) through TFC is presented and some differences between the circular and elliptic problems are discussed. The application of TFC to solve the temporary gravitational capture based on the CR3BP, considering backward integration, is presented under different formulations, including inertial and rotating frames, as well as initial and boundary value problems. Error comparisons among these cases are provided and the best strategies for solving the capture problem, depending on the need, are discussed.

Resumen

Este artículo presenta aplicaciones de la Teoría de Conexiones Funcionales (Theory of Functional Connections, TFC) para la resolución de problemas en mecánica celeste, con especial énfasis en la captura gravitacional temporal. El marco univariado de la TFC se emplea para resolver ecuaciones diferenciales de segundo orden. Se presenta la formulación matemática para la solución del problema de dos cuerpos y del problema restringido de tres cuerpos circular (CR3BP, por sus siglas en inglés) mediante TFC, y se discuten algunas diferencias entre los casos circular y elíptico. Asimismo, se aplica la TFC al estudio de la captura gravitacional temporal basada en el CR3BP, considerando integración hacia atrás, bajo distintas formulaciones que incluyen marcos de referencia inercial y rotante, así como problemas de valores iniciales y de contorno. Se presentan comparaciones de error entre estos casos y se discuten las estrategias más adecuadas para resolver el problema de captura según los requerimientos de cada aplicación.

Corresponding author: G. Afonso Siqueli *E-mail address:* guilhermesiqueli@protonmail.com
Received: April 28, 2025 **Accepted:** July 4, 2025

1. Introduction

Orbital propagation is fundamental to the study of problems in celestial mechanics. Several methods can be used, depending on the system in question, from the two-body problem (2BP), the circular (or elliptical) restricted three-body problem (CR3BP/ER3BP), to a generalization of the n-body problem. Classically, these problems are solved via numerical integration, with increasingly sophisticated integrators.

One of these problems in celestial mechanics is the temporary gravitational capture in a system composed of three bodies, in which a body B_3 of mass m_3 is captured by a body B_1 of mass m_1 and has its motion disturbed by a body B_2 of mass m_2. When $m_2 > m_1$, with the mass m_3 being negligible in relation to the others and the eccentricity of the orbit of body B_1 around B_2 being sufficiently small, this problem can be solved by CR3BP.

The term *gravitational capture* refers to the process in which a spacecraft transitions from a hyperbolic trajectory (unbound orbit) to an elliptical trajectory (bound orbit) around a celestial body owing to the gravitational influence of other celestial bodies. Several studies have been conducted on this topic, particularly related to missions to the Moon, which was the first motivation for these studies (Belbruno & Miller, 1993; Belbruno, 1987; Circi & Teofilatto, 2001; Yamakawa et al., 1993; Yamakawa et al., 1992; Dahlke, 1998, Investigation of lunar ballistic capture transfer trajectories; Yamakawa & Yawaguchi, 1993).

The general idea is to send a spacecraft on a longer trajectory such that when approaching the desired celestial body, it suffers a small but constant force from the gravity field of one or more celestial bodies, and when it reaches the final celestial body, it has a negative two-body energy with respect to this body (Belbruno et al., 2008; Belbruno, 2004; Belbruno et al., 2010; García & Gómez, 2007).

There is no need to use fuel for that part of the maneuver. However, this capture is never permanent, and after some time, the spacecraft will escape again from the celestial body. The use of this technique is usually combined with fuel based maneuvers that complete the capture during the time that the two body energy is negative, so there is a saving in the fuel consumption. After the first studies on lunar missions, other applications were considered (Li & Sun, 2015; Topputo & Belbruno, 2009, 2015).

This maneuver typically results in much longer transfer times, which is a penalty for the gains in fuel consumption. Some studies have examined this point (Machuy et al., 2007; Neto & de Almeida Prado, 1998).

In general, gravitational capture is modeled based on the three-body problem, either in its circular or elliptical form, and solved through numerical integration. Given the initial conditions at the end of the capture, numerical integration backward in time is performed to calculate the trajectory around the primary until the third body crosses the sphere of influence of this primary (a condition that characterizes the capture). The solution obtained using this method requires sophisticated numerical integrators that allow for accurate numerical integration.

The purpose of this paper is to provide a unified framework to obtain analytically approximated solutions of non-homogeneous linear differential equations that represent the dynamics of the CR3BP, without other perturbations, subject to a set of two constraints, using the Theory of Functional Connections (TFC). This method can be found in the original paper by Mortari (2017a) and is presented in detail in §2. The first papers on TFC were published in 2017 (Mortari, 2017b; Johnston et al., 2020).

A least-squares solution is provided to ensure a high-accuracy solution.

2. TFC Method for Solving Second-Order Differential Equations

This section presents the TFC method applied to the solution of Second-Order Differential Equations (SODE) using the least-squares method.

Given a linear or nonlinear SODE, with constant or variable coefficients, homogeneous or non-homogeneous, as described by Eq. 1, a linear transformation can be applied to the independent variable of this equation (in this case the time t) so that the new independent variable is defined over the interval of [-1 1]. A new independent variable, denoted by λ, is introduced through the linear transformation given by Eq. 2.

$$\mathbf{f}_2(t)\ddot{\mathbf{y}}(t) + \mathbf{f}_1(t)\dot{\mathbf{y}}(t) + \mathbf{f}_0(t)\mathbf{y}(t) = \mathbf{f}(t), \tag{1}$$

$$\lambda = \frac{\lambda_f - \lambda_0}{t_f - t_0}(t - t_0) + \lambda_0. \tag{2}$$

In Eq. 1 the terms $\mathbf{f}_2(t)$, $\mathbf{f}_1(t)$ and $\mathbf{f}_0(t)$ are coefficients of the SODE. The function $\mathbf{y}$(t) represents the dependent variable, whereas t is the independent variable, corresponding to time in the context of gravitational capture studies. The term $\mathbf{f}(t)$ denotes the forcing term.

In Eq. 2, λ_f and λ_0 represent the bounds of the time interval over which the SODE is analyzed, and t is an arbitrary time within the domain of the original independent variable t. Similarly, t_f and t_0 denote the bounds of the new independent variable λ, namely -1 and 1, respectively, when orthogonal polynomials are considered, where λ is an arbitrary time variable within the scope of this transformed independent variable.

Consequently, the original differential equation is transformed as follows: 3, where c is defined by Eq. 4:

$$c^2\mathbf{f}_2(\lambda)\mathbf{y}''(\lambda) + c\mathbf{f}_1(\lambda)\mathbf{y}'(\lambda) + \mathbf{f}_0(\lambda)\mathbf{y}(\lambda) = \mathbf{f}(\lambda), \tag{3}$$

$$c = \frac{\lambda_f - \lambda_0}{t_f - t_0}. \tag{4}$$

The first and second derivatives of $\mathbf{y}(\lambda)$ with respect to λ are defined in Eqs. 5 and 6, respectively:

$$\frac{d}{d\lambda}\mathbf{y}(\lambda) = \mathbf{y}'(\lambda), \tag{5}$$

$$\frac{d^2}{d\lambda^2}\mathbf{y}(\lambda) = \mathbf{y}''(\lambda). \tag{6}$$

Eq. 3 can be solved using a constrained expression (Mortari, 2017a) given by Eq. 9, considering the initial conditions, as specified in Eqs. 7 and 8:

$$y(t = 0) = y(\lambda = -1) = y_0, \tag{7}$$

$$\dot{y}(t = 0) = \dot{y}_0 = cy'(\lambda = -1) = y'_0, \tag{8}$$

$$\mathbf{y}(\lambda) = \mathbf{g}(\lambda) + \nu_1\mathbf{p}(\lambda) + \nu_2\mathbf{q}(\lambda), \tag{9}$$

where y_0 is the initial position, y'_0 is the initial velocity, $\mathbf{p}(\lambda)$ and $\mathbf{q}(\lambda)$ are assigned functions, $\mathbf{g}(\lambda)$ is an unknown free function, and ν_1 and ν_2 are unknown coefficients to be determined.

The first derivative of Eq. 9 is expressed by Eq. 10:

$$\mathbf{y}'(\lambda) = \mathbf{g}'(\lambda) + \nu_1\mathbf{p}'(\lambda) + \nu_2\mathbf{q}'(\lambda), \tag{10}$$

where $\mathbf{y}'(\lambda)$, $\mathbf{g}'(\lambda)$, $\mathbf{p}'(\lambda)$ and $\mathbf{q}'(\lambda)$ denote the respective first derivatives of $\mathbf{y}(\lambda)$, $\mathbf{g}(\lambda)$, $\mathbf{p}(\lambda)$ and $\mathbf{q}(\lambda)$ with respect to λ.

Therefore, it is possible to write the system in the form of Eq. 11. It can be solved for ν_1 and ν_2 according to Eq. 12, based on the initial conditions:

$$\begin{bmatrix}\mathbf{y}(\lambda)\\ \mathbf{y}'(\lambda)\end{bmatrix} = \begin{bmatrix}\mathbf{p}(\lambda) & \mathbf{q}(\lambda)\\ \mathbf{p}'(\lambda) & \mathbf{q}'(\lambda)\end{bmatrix}\begin{bmatrix}\nu_1\\ \nu_2\end{bmatrix} = \begin{bmatrix}\mathbf{g}(\lambda)\\ \mathbf{g}'(\lambda)\end{bmatrix}, \tag{11}$$

$$\begin{bmatrix}\nu_1\\ \nu_2\end{bmatrix} = \begin{bmatrix}p_0 & q_0\\ p'_0 & q'_0\end{bmatrix}^{-1}\begin{bmatrix}y_0 - g_0\\ y'_0 - g'_0\end{bmatrix} = \begin{bmatrix}Y_0\\ Y'_0\end{bmatrix} - \begin{bmatrix}h_{11} & h_{12}\\ h_{21} & h_{22}\end{bmatrix}\begin{bmatrix}g_0\\ g'_0\end{bmatrix}. \tag{12}$$

In Eq. 12 p_0, q_0, p'_0, q'_0, y_0, y'_0, g_0 and g'_0 correspond to the respective functions $\mathbf{p}(\lambda)$, $\mathbf{q}(\lambda)$, $\mathbf{p}'(\lambda)$, $\mathbf{q}'(\lambda)$, $\mathbf{y}(\lambda)$, $\mathbf{y}'(\lambda)$, $\mathbf{g}(\lambda)$, $\mathbf{g}'(\lambda)$ evaluated at the initial time.

By substituting ν_1 and ν_2 in the constrained expression 9, Eq. 13 is obtained:

$$\mathbf{y}(\lambda) = \mathbf{g}(\lambda) + \left[Y_0 - (h_{11}g_0 + h_{12}g'_0)\right]\mathbf{p}(\lambda) + \left[Y'_0 - (h_{21}g_0 + h_{22}g'_0)\right]\mathbf{q}(\lambda), \tag{13}$$

where Y_0, Y'_0, h_{11}, h_{12}, h_{21} and h_{22} are given by the result of Eq. 12.

Eq. 13 can be further simplified as shown in Eq. 14, where $\boldsymbol{\varphi}_1$ and $\boldsymbol{\varphi}_2$ are given by Eqs. 15 and 16, respectively:

$$\mathbf{y}(\lambda) = \mathbf{g}(\lambda) - \boldsymbol{\varphi}_1 g_0 - \boldsymbol{\varphi}_2 g'_0 + Y_0\mathbf{p}(\lambda) + Y'_0\mathbf{q}(\lambda), \tag{14}$$

$$\boldsymbol{\varphi}_1 = h_{11}\mathbf{p}(\lambda) + h_{21}\mathbf{q}(\lambda), \tag{15}$$

$$\boldsymbol{\varphi}_2 = h_{12}\mathbf{p}(\lambda) + h_{22}\mathbf{q}(\lambda). \tag{16}$$

By differentiating Eq. 14 and substituting in Eq. 3, the differential equation assumes the form of Eq. 17, where $\boldsymbol{\chi}_1(\lambda)$ and $\boldsymbol{\chi}_2(\lambda)$ are given by Eqs. 18 and 19 and $\boldsymbol{\upsilon}(\lambda)$ is given by Eq. 20:

$$c^2\mathbf{f}_2(\lambda)\mathbf{g}''(\lambda) + c\mathbf{f}_1(\lambda)\mathbf{g}'(\lambda) + \mathbf{f}_0(\lambda)\mathbf{g}(\lambda) - \boldsymbol{\chi}_1(\lambda)g_0 - \boldsymbol{\chi}_2(\lambda)g'_0 = \boldsymbol{\upsilon}(\lambda), \tag{17}$$

$$\boldsymbol{\chi}_1(\lambda) = c^2\mathbf{f}_2(\lambda)\boldsymbol{\varphi}_1''(\lambda) + c\mathbf{f}_1(\lambda)\boldsymbol{\varphi}_1'(\lambda) + \mathbf{f}_0(\lambda)\boldsymbol{\varphi}_1(\lambda), \quad (18)$$

$$\boldsymbol{\chi}_2(\lambda) = c^2\mathbf{f}_2(\lambda)\boldsymbol{\varphi}_2''(\lambda) + c\mathbf{f}_1(\lambda)\boldsymbol{\varphi}_2'(\lambda) + \mathbf{f}_0(\lambda)\boldsymbol{\varphi}_2(\lambda), \quad (19)$$

$$\begin{aligned}\boldsymbol{\upsilon}(\lambda) = \mathbf{f}(\lambda) - c^2\mathbf{f}_2(\lambda)\left[Y_0 p''(\lambda) + Y_0' q''(\lambda)\right] \\ -c\mathbf{f}_1(\lambda)\left[Y_0 p'(\lambda) + Y_0' q'(\lambda)\right] - \mathbf{f}_0(\lambda)\left[Y_0 p(\lambda) + Y_0' q(\lambda)\right]\mathbf{y}(\lambda).\end{aligned} \quad (20)$$

The free function $\mathbf{g}(\lambda)$ can be expressed as a linear combination of m basis functions $\mathbf{h}(\lambda)$, enabling the system defined by Eq. 17 to be reformulated in matrix form as shown in Eq. 22. These basis functions can conveniently be Legendre or Chebyshev polynomials (Mortari, 2017a). This is a common consideration in TFC-related literature:

$$\mathbf{g}(\lambda) = \boldsymbol{\sigma}^T\mathbf{h}(\lambda), \quad (21)$$

$$\mathrm{Y}\boldsymbol{\sigma}^T = \boldsymbol{\upsilon}(\lambda). \quad (22)$$

In Eqs. 21 and 22, σ is a vector of coefficients to be calculated in order to approximate the solution of the SODE for each of the N equations, corresponding to the N evaluated points.

Each element of the matrix Y is given by Eq. 23 and each element of the vector υ is given by Eq. 20 for $\lambda = \lambda_i$. Note that the matrix Y in Eq. 22, is a matrix $m \times N$, where m is the number of terms of the polynomial series used in the calculation and N is the number of time instants evaluated (segmentation of λ). The values at each of these instants (λ_i) can be obtained from Eq. 24:

$$\mathrm{Y}_{ij} = c^2\mathbf{f}_2(\lambda)\mathbf{h}''(\lambda) + c\mathbf{f}_1(\lambda)\mathbf{h}'(\lambda) + \mathbf{f}_0(\lambda)\mathbf{h}(\lambda) - \boldsymbol{\chi}_1(\lambda)g_0 - \boldsymbol{\chi}_2(\lambda)g_0', \quad (23)$$

$$\lambda_i = -\cos\frac{i\pi}{N}. \quad (24)$$

The N values calculated using Eq. 24 are the optimal values for λ (Lanczos, 1957; Wright, 1964; Johnston et al., 2020).

Eq. 23 presents the ij-th element of the matrix Y, where $(1 < i < N)$ and $(1 < j < m)$. Indeed, this matrix arises from the fact that the functions $\mathbf{h}$ are polynomials. Therefore, the term h_{ij} is associated with the instant (λ_i) and corresponds to the ij-th term of the polynomial series. It is important to note that the basis functions must be linearly independent of the support functions $\mathbf{p}(\lambda)$ and $\mathbf{q}(\lambda)$ (Mortari, 2017a; Mortari et al., 2019). Consequently, because the first two terms of the polynomial series have already been used for the support functions, these terms cannot be considered in the computation of the functions $\mathbf{h}(\lambda)$ and their derivatives.

Therefore, at this point, it is possible to obtain a solution to Eq. 3: by solving the system given by Eq. 22, the vector $\boldsymbol{\sigma}$ is obtained and the free function $g(\lambda)$ can be calculated through Eq. 21. Consequently, Eq. 14, which represents the solution to the SODE, is fully defined.

This initial solution, obtained through the calculation of $\boldsymbol{\sigma}$, which we may refer to as $\boldsymbol{\sigma}_0$, cannot achieve the desired accuracy specified by the user. The loss function (Eq. 25) is also known as the residual vector of the differential equation. The error in the least-squares method corresponds to the norm of this residual, as given by Eq. 26:

$$\mathcal{L}_k(\lambda) = \mathrm{Y}\boldsymbol{\sigma} - \boldsymbol{\upsilon}(\lambda), \quad (25)$$

$$\varepsilon = |\mathcal{L}_k(\lambda)|. \quad (26)$$

Machine-level accuracy can be achieved by solving the problem using the TFC method with the least squares method (Mortari et al., 2019; Johnston et al., 2020). However, in cases where the desired level is not achieved in the first step, that is, with the calculation of $\boldsymbol{\sigma}_0$, it is possible to reduce the errors through a linearization of the differential equation around the initial solution ($\boldsymbol{\sigma}_0$), as given in Eq. 27, where $\frac{\partial\mathcal{L}}{\partial\boldsymbol{\sigma}}$ is given by Eq. 28. Nevertheless, this refinement is limited by factors such as the number of polynomials considered in the calculation (m) and the number of time instants evaluated (N).

$$\mathcal{L}_k + \left(\frac{\partial\mathcal{L}}{\partial\boldsymbol{\sigma}}\right)_k^T(\boldsymbol{\sigma}_{k+1} - \boldsymbol{\sigma}_k) = 0, \quad (27)$$

$$\frac{\partial\mathcal{L}}{\partial\boldsymbol{\sigma}} = \sum_{i=0}^{n}\left(\frac{\partial\mathcal{L}}{\partial\mathbf{y}^{(i)}}\frac{\partial\mathbf{y}^{(i)}}{\partial\boldsymbol{\sigma}}\right). \quad (28)$$

In Eqs. 27 and 28 the term $\frac{\partial\mathcal{L}}{\partial\boldsymbol{\sigma}}$ is the Jacobian, $\boldsymbol{\sigma}_{k+1}$ is the current value of $\boldsymbol{\sigma}$, $\boldsymbol{\sigma}_{k+1}$ is the value of $\boldsymbol{\sigma}$ calculated from k_{th} iteration.

Therefore, the linearization process is essential for refining the solution iteratively. This approach allows controlled convergence of the method by updating the coefficients $\boldsymbol{\sigma}$ while recognizing that the achievable precision is inherently limited by the chosen polynomial basis size and discretization resolution.

Thus, the combination of the constrained expression formulation provided by the TFC method with the linearization technique, provides a systematic framework for solving SODE under various conditions, ensuring accuracy in practical applications, and can be directly applied to the computation of temporary gravitational capture problems.

3. TWO-BODY PROBLEM SOLVING VIA THEORY OF FUNCTIONAL CONNECTIONS

The temporary gravitational capture problem involves determining the motion of a body orbiting a primary body and subject to disturbance by other bodies. When only one disturbing body is considered, the problem can be modeled using the three-body problem. However, the motion of the primary and secondary bodies (bodies B_1 and B_2) occur around their barycenter and can be determined from the two-body problem (2BP). The motion is analyzed in this section.

The two-body problem is quite simple, well documented in the literature, and has an analytical solution. Since 2BP can be solved analytically, TFC is not necessary to solve it. However, some interesting preliminary conclusions regarding TFC applications can be obtained by solving the 2BP via TFC. A representative application of the TFC in the context of celestial mechanics can be found in de Almeida Junior et al. (2021).

The motion of body B_2 around body B_1 can be represented by the differential equation (Eq. 29):

$$\ddot{\mathbf{r}} = -\frac{\mu_1}{|r|^3}\mathbf{r}, \quad (29)$$

where μ_1 is the gravitational constant of body B_1, $\mathbf{r}$ is the vector radius between bodies B_1 and B_2 and $\ddot{\mathbf{r}}$ is the respective acceleration.

The solution to this equation is given by Eq. 30:

$$\mathbf{r} = \frac{a\left(1-e^2\right)}{1+e\cos f}, \tag{30}$$

where a is the semi-major axis, e is the eccentricity and f is the true anomaly. Then, using Kepler's equation (Eq. 31):

$$M = nt = u - e\sin u, \tag{31}$$

where M is the mean anomaly, u is the eccentric anomaly, n is the mean motion and t is the time.

The conversion between the eccentric anomaly and the true anomaly is given by Eq. 32:

$$\tan^2\frac{f}{2} = \frac{1+e}{1-e}\tan^2\frac{u}{2}. \tag{32}$$

It is possible to solve this problem through TFC, initially identifying the SODE coefficients (according to Eq. 1) as being $\mathbf{f}_2(t) = 1$, $\mathbf{f}_1(t) = 0$, $\mathbf{f}_0(t) = \mu\mathbf{r}/|\mathbf{r}|^3$ and $\mathbf{f}(t) = 0$. Here, as in the introduction, we present the initial value problem, in which, given the initial position (Eq. 33) and the initial velocity (Eq. 34), we seek to calculate the positions and velocities for a later time.

$$\mathbf{r}(t=0) = \mathbf{r}(\lambda=-1) = r_0 \tag{33}$$

$$\dot{\mathbf{r}}(t=0) = \dot{\mathbf{r}}_0 = c\mathbf{r}'(\lambda=-1) = r_0' \tag{34}$$

In Eq. 33 $\dot{\mathbf{r}}$ represents the first derivative with respect to t, and $\mathbf{r}'$ represents the first derivative with respect to λ.

The proposed constrained expression is analogous to Eq. 9, given by Eq. 35.

$$\mathbf{r}(\lambda) = \mathbf{g}(\lambda) + \nu_1\mathbf{p}(\lambda) + \nu_2\mathbf{q}(\lambda) \tag{35}$$

Applying the TFC we obtain the Eq. 36,

$$\mathbf{r}(\lambda) = \boldsymbol{\sigma}^T\left[\mathbf{h}(\lambda) - \mathbf{h}_0 - (1+\lambda)\mathbf{h}_0'\right] + \mathbf{r}_0 + (1+\lambda)\mathbf{r}_0' \tag{36}$$

which calculates the value of $\mathbf{r}(\lambda)$ for every desired time value (dimensionless in the range of the λ variable). The matrix Y and the vector υ are given by Eqs. 37 and 38.

$$\mathrm{Y}_{ij} = c^2\mathbf{h}_j''(\lambda_i) + \frac{\mu}{\mathbf{r}^3}(1+\lambda)\left[\mathbf{h}_j(\lambda_i) - \mathbf{h}_0 - (1+\lambda)\mathbf{h}_0'\right] \tag{37}$$

$$\upsilon_{ij} = \frac{\mu}{\mathbf{r}^3}\left[(r_0 + r_0') + r_0'\lambda\right] \tag{38}$$

The assembly of the matrix Y follows the same logic presented in Eq. 23.

In a two-dimensional 2BP, that is, in the case where the trajectory is calculated in the orbital plane only, two variables are calculated (x and y). It is worth noting the difference between the cases of circular and elliptical orbits. The problem of circular orbits can be solved in different ways:

- If it is not assumed that $\mathbf{r}(t)$ is constant before to start the calculations, the problem can be solved in two different ways:
  - In a decoupled form, considering the variables x and y independently and assembling two systems, as shown in Eq. 40, and solving them independently,
  - or in a coupled form, solving one system as shown in Eq. 41, with both variables together,

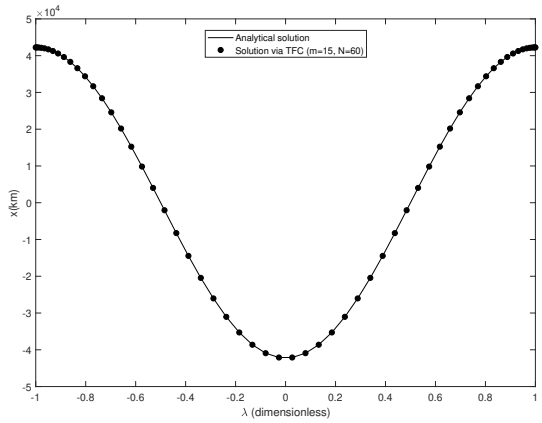

Figure 1. Temporal evolution traces of the circular orbital trajectory on the x-axis, in the two-body problem, for the analytical solution (continuous line) and the solution obtained by TFC (black circles).

$$\begin{aligned}\boldsymbol{\Upsilon}_x\boldsymbol{\sigma}_{0x}^T &= \upsilon_x\\ \boldsymbol{\Upsilon}_y\boldsymbol{\sigma}_{0y}^T &= \upsilon_y\end{aligned} \tag{39}$$

$$\boldsymbol{\Upsilon} = \begin{bmatrix}\boldsymbol{\Upsilon}_x & 0\\ 0 & \boldsymbol{\Upsilon}_y\end{bmatrix} \qquad \boldsymbol{\sigma} = \begin{bmatrix}\boldsymbol{\sigma}_{0x}\\ \boldsymbol{\sigma}_{0y}\end{bmatrix} \qquad \upsilon = \begin{bmatrix}\upsilon_x\\ \upsilon_y\end{bmatrix} \tag{40}$$

  where the subscript x indicates that the respective matrices and vectors pertain to the calculation of $x(\lambda)$, and the subscript y pertains to the calculation of $y(\lambda)$.
- If it is assumed that $\mathbf{r}(t)$ is constant before to start the calculations, the problem can be solved for only one variable x or y (one of the Eqs. 40). The set of $\boldsymbol{\sigma}$ is valid for both variables. Of course, assuming this premise means that there is no need to perform the calculations; however, in any case, this situation is presented for educational purposes to demonstrate the internal consequences of the method.

The trajectories on the x- and y-axes are shown in Figures 1 and 2, respectively, and the complete orbit is shown in Figure 3, for a bi-dimensional geostationary circular orbit with the following initial conditions: position (42245 0 0) km, velocity (0 3.0722) km/s, and considering 15 Legendre polynomial terms ($m = 15$) in the calculation, with evaluations every 60 instants of time ($N = 60$). The calculated error was 7.5×10^{-12}, which was sufficiently low.

This is a very important test for the TFC. The results are very close to the analytical solutions, which demonstrates the efficiency of the TFC.

The problem of elliptical orbits can only be solved in a coupled form by solving the system given by Eq. 41, with both variables at the same time. As an example, a situation was simulated with orbital elements equal to those of the geocentric orbit, but with an eccentricity of 0.1. The initial conditions then become: position (38020, 0) km and velocity (0, 3.3964) km/s. The simulation was segmented into four intervals of 6 hours each, because the

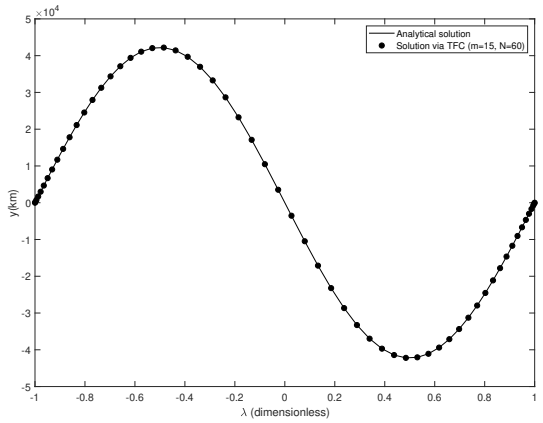

Figure 2. Temporal evolution of the circular orbital trajectory on the y-axis in the 2BP.

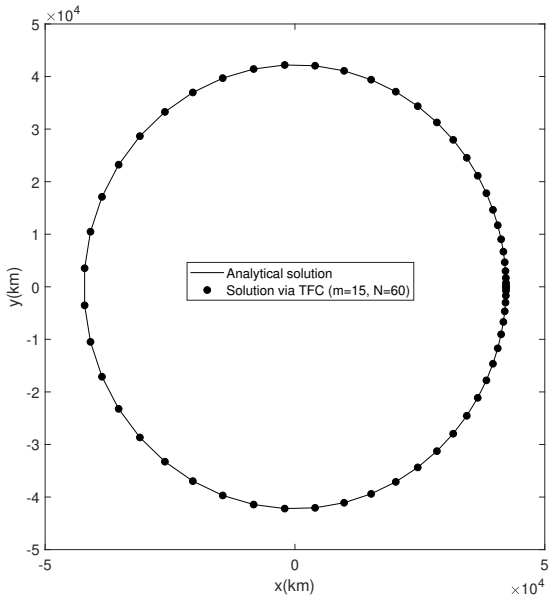

Figure 3. Circular orbit trajectory in the 2BP: TFC results vs analytical solution.

TFC presents some problems when dealing with closed and/or periodic orbits. Therefore, Figures 4 and 5 present four quadrants, each equivalent to a 6-hour simulation. A total of 15 Legendre polynomial terms were considered ($m = 15$), and 30 time instants were evaluated ($N = 30$) for each segment. The errors obtained for $\boldsymbol{\sigma}_0$ were in the order of 10^{-7} and, with 3 iterations, using the DE linearization proposed in Eqs. 27 and 28, errors in the order of 10^{-12} were obtained.

The loss function and its derivative with respect to $\boldsymbol{\sigma}$ are given by Eqs. 41 and 42, respectively.

$$\mathcal{L} = c^2\mathbf{r}'' + \frac{\mu}{||\mathbf{r}||^3}\mathbf{r} \tag{41}$$

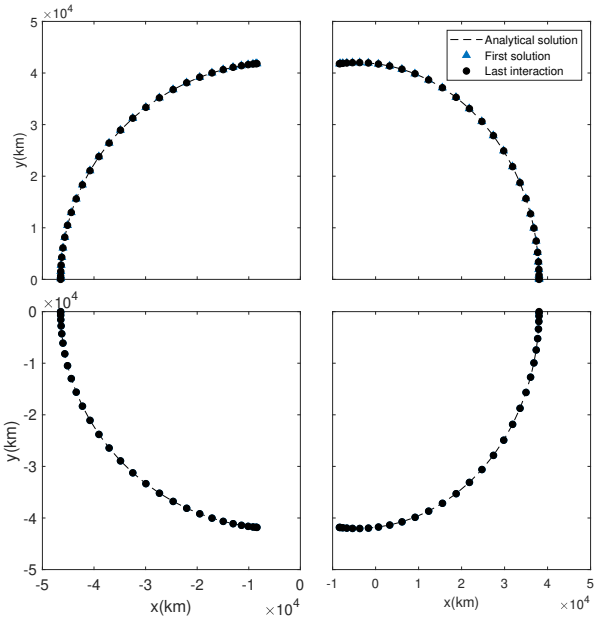

Figure 4. Elliptical orbit trajectory in the two-body problem: TFC results vs analytical solution.

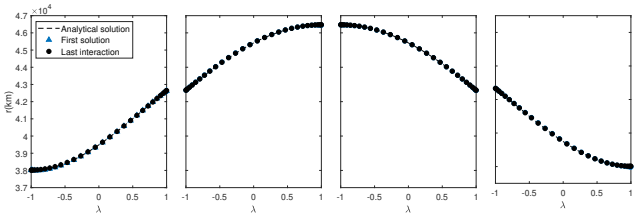

Figure 5. Temporal evolution of radius vector $\mathbf{r}(\lambda)$ in a elliptical orbital trajectory in the 2BP: TFC results vs analytical solution.

$$\mathcal{L} = c^2\boldsymbol{\sigma}^T\mathbf{h}'' + \frac{\mu}{||\mathbf{r}||^3}\left\{\boldsymbol{\sigma}^T\left[\mathbf{h}(\lambda) - \mathbf{h}_0 - (1+\lambda)\mathbf{h}_0'\right] + \mathbf{r}_0 + (1+\lambda)\mathbf{r}_0'\right\} \tag{42}$$

The complete elliptical orbit is illustrated in Figure 4 and the radius vector $\mathbf{r}(\lambda)$ is illustrated in Figure 5. Again, the results are very close to the analytical solutions, and the behavior of the elliptical orbit is correctly demonstrated.

4. CIRCULAR RESTRICTED THREE-BODY PROBLEM SOLVED VIA THEORY OF FUNCTIONAL CONNECTIONS

The problem of temporary gravitational capture addressed in this study is modeled based on the circular restricted three-body problem (CR3BP). In this model, the movement of the primaries is considered around their barycenter, and the movement of body B_3 around the primary is studied, as illustrated in Figure 6. Body B_1 is called the primary body, whereas body B_2 is called the secondary or disturbing body.

The movement of body B_3 can be calculated in both the inertial reference system (ξ-η) and the rotating system (x-y), with the same origin of the inertial system that rotates with an angular velocity equal to the movement of bodies B_1 and B_2 around the

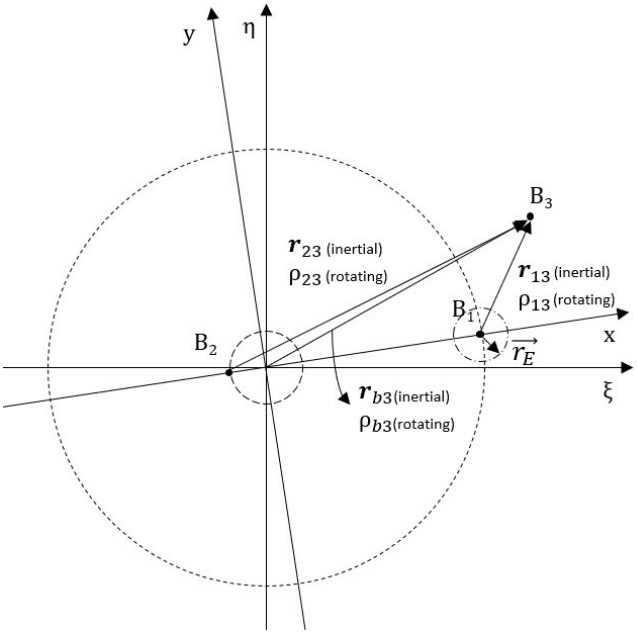

Figure 6. Schematic model of the restricted circular three-body problem (inertial and rotating reference frames).

barycenter. In other others, the primary and secondary do not move in the rotating system.

4.1. Solving the CR3BP initial value problem, with equations in the inertial frame, via TFC

The equations of motion that describe the trajectory of body B_3 in the inertial system of reference are given by Eqs 43 and 44 for ξ and η respectively (ξ and η are components of vector ρ_{23} illustrated in Figure 6). These equations are already formatted as Eq. 1 and it is easy to identify the DE coefficients (Eqs. 46 and 47).

$$\ddot{\xi}+\left[\frac{\mu}{|\rho_{13}|^3}+\frac{(1-\mu)}{|\rho_{23}|^3}\right]\xi=-\left[\frac{-\mu(1-\mu)\cos(\tau)}{|\rho_{13}|^3}+\frac{(1-\mu)\mu\cos(\tau)}{|\rho_{23}|^3}\right] \tag{43}$$

$$\ddot{\eta}+\left[\frac{\mu}{|\rho_{13}|^3}+\frac{(1-\mu)}{|\rho_{23}|^3}\right]\eta=-\left[\frac{-\mu(1-\mu)\sin(\tau)}{|\rho_{13}|^3}+\frac{(1-\mu)\mu\sin(\tau)}{|\rho_{23}|^3}\right] \tag{44}$$

where ρ_{13} and ρ_{23} are given by Eq. 45.

$$\begin{aligned}|\rho_{13}|^2&=[\xi_{b3}-(1-\mu)^*\cos\tau]^2+[\eta_{b3}-(1-\mu)^*\sin\tau]^2+(\zeta_{b3})^2\\ |\rho_{23}|^2&=(\xi_{b3}+\mu^*\cos\tau)^2+(\eta_{b3}+\mu^*\sin\tau)^2+(\zeta_{b3})^2\end{aligned} \tag{45}$$

In Eqs. 43, 43 and 45, μ is the gravitational constant, ρ_{13} is the distance from body B_1 (primary) to body B_3, ρ_{23} is the distance from body B_2 (secondary) to body B_3, and τ is the time. All the variables were dimensionless.

$$\begin{aligned}f_{2\xi}&=1\\ f_{1\xi}&=0\\ f_{0\xi}&=\frac{\mu}{|\rho_{13}|^3}+\frac{(1-\mu)}{|\rho_{23}|^3}\\ f_{\xi}&=-\left[\frac{-\mu(1-\mu)\cos(\tau)}{|\rho_{13}|^3}+\frac{(1-\mu)\mu\cos(\tau)}{|\rho_{23}|^3}\right]\end{aligned} \tag{46}$$

$$\begin{aligned}f_{2\eta}&=1\\ f_{1\eta}&=0\\ f_{0\eta}&=\frac{\mu}{|\rho_{13}|^3}+\frac{(1-\mu)}{|\rho_{23}|^3}\\ f_{\eta}&=-\left[\frac{-\mu(1-\mu)\sin(\tau)}{|\rho_{13}|^3}+\frac{(1-\mu)\mu\sin(\tau)}{|\rho_{23}|^3}\right]\end{aligned} \tag{47}$$

In Eqs. 46 and 47, $f_{2\xi}$, $f_{1\xi}$, $f_{0\xi}$ and f_{ξ} are the equivalent values of $\mathbf{f}_2(t)$, $\mathbf{f}_1(t)$, $\mathbf{f}_0(t)$ and $\mathbf{f}(t)$, presented in Eq. 1, for Eq. 43 and $f_{2\eta}$, $f_{1\eta}$, $f_{0\eta}$ and f_{η} are the equivalent values for Eq. 44.

Following the step-by-step process presented previously for TFC, the following expressions can be obtained for the matrix Y and the vector υ for the coordinates ξ (Eqs. 48 and 49) and η (Eqs. 50 and 51), respectively:

$$\mathrm{Y}_{\xi_{ij}}=c^2\mathbf{h}''(\lambda)+\mathbf{f}_{0\xi}(\lambda)\left[\mathbf{h}(\lambda)-h_0-(1+\lambda)h_0'\right] \tag{48}$$

$$\upsilon_{\xi_i}(\lambda)=f_{\xi}-f_{0\xi}\left[\xi_0+(1+\lambda)\frac{\dot{\xi}_0}{c}\right] \tag{49}$$

$$\mathrm{Y}_{\eta_{ij}}=c^2\mathbf{h}''(\lambda)+\mathbf{f}_{0\eta}(\lambda)\left[\mathbf{h}(\lambda)-h_0-h_0'\right] \tag{50}$$

$$\upsilon_{\eta_i}(\lambda)=f_{\eta}-f_{0\eta}\left[\eta_0+(1+\lambda)\frac{\dot{\eta}_0}{c}\right] \tag{51}$$

where $\mathrm{Y}_{\xi_{ij}}$ is the ij-th element of the matrix Y_{ξ}, which corresponds to the matrix Y used for the calculation of $\xi(\lambda)$, υ_{ξ_i} is the i-th element of the vector $\boldsymbol{\upsilon}_{\xi}$, which corresponds to the vector $\boldsymbol{\upsilon}$ used for the calculation of $\xi(\lambda)$ and $\mathrm{Y}_{\eta_{ij}}$ and $\upsilon_{\eta_i}(\lambda)$ are the equivalent values for $\eta(\lambda)$.

The constrained expressions become Eqs. 52 and 53,

$$\xi(\lambda)=\boldsymbol{\sigma}_{\xi}\left[\mathbf{h}(\lambda)-h_0-(1+\lambda)\,h_0'\right]+\xi_0+\frac{\dot{\xi}_0}{c}(1+\lambda) \tag{52}$$

$$\eta(\lambda)=\boldsymbol{\sigma}_{\eta}\left[\mathbf{h}(\lambda)-h_0-(1+\lambda)\,h_0'\right]+\eta_0+\frac{\dot{\eta}_0}{c}(1+\lambda) \tag{53}$$

where, h_0 and h_0' are, respectively, $\mathbf{h}(\lambda)$ and $\mathbf{h}'(\lambda)$ calculated for $\lambda=-1$. The quantities $\dot{\xi}_0$ and $\dot{\eta}_0$ are the components of the initial velocity.

The loss functions for ξ and η are given, respectively, by Eqs. 54 and 55,

$$\mathcal{L}_\xi(\xi,\xi'',\eta,\boldsymbol{\sigma}_\xi,\boldsymbol{\sigma}_\eta) = c^2\xi'' + \frac{\mu\left[\xi-\xi_{b1}\right]}{\left[\left(\xi-\xi_{b1}\right)^2+\left(\eta-\eta_{b1}\right)^2\right]^{3/2}} + \frac{(1-\mu)\left[\xi-\xi_{b2}\right]}{\left[\left(\xi-\xi_{b2}\right)^2+\left(\eta-\eta_{b2}\right)^2\right]^{3/2}} \tag{54}$$

$$\mathcal{L}_\eta(\eta,\eta'',\xi,\boldsymbol{\sigma}_\eta,\boldsymbol{\sigma}_\xi) = c^2\eta'' + \frac{\mu\left[\eta-\eta_{b1}\right]}{\left[\left(\xi-\xi_{b1}\right)^2+\left(\eta-\eta_{b1}\right)^2\right]^{3/2}} + \frac{(1-\mu)\left[\eta-\eta_{b2}\right]}{\left[\left(\xi-\xi_{b2}\right)^2+\left(\eta-\eta_{b2}\right)^2\right]^{3/2}} \tag{55}$$

where ξ_{b1} and η_{b1} are the equivalent components ξ and η for body B_1, ξ_{b2} and η_{b2} are the equivalent components ξ and η for body B_2, and $\mathcal{L}_\xi$ and $\mathcal{L}_\eta$ are the loss functions for each component individually.

The Jacobian (J) is given by Eq. 56 and its components are presented in Eqs. 57, 58, 59 and 60.

$$J = \left(\frac{\partial\mathcal{L}}{\partial\boldsymbol{\sigma}}\right)_k^T = \begin{bmatrix} \frac{\partial\mathcal{L}_\xi}{\partial\boldsymbol{\sigma}_\xi} & \frac{\partial\mathcal{L}_\eta}{\partial\boldsymbol{\sigma}_\xi} \\ \frac{\partial\mathcal{L}_\xi}{\partial\boldsymbol{\sigma}_\eta} & \frac{\partial\mathcal{L}_\eta}{\partial\boldsymbol{\sigma}_\eta} \end{bmatrix} \tag{56}$$

$$\frac{\partial\mathcal{L}_\xi}{\partial\boldsymbol{\sigma}_\xi} = c^2\mathbf{h}'' + \left[-\frac{3\mu\left(\xi-\xi_{b1}\right)^2}{\rho_{13}^5} + \frac{\mu}{\rho_{13}^5} - \frac{3(1-\mu)\left(\xi-\xi_{b2}\right)^2}{\rho_{23}^5} + \left[\frac{1-\mu}{\rho_{23}^5}\right]\right]\left[\mathbf{h} - h_0 - (1+\lambda)h_0'\right] \tag{57}$$

$$\frac{\partial\mathcal{L}_\xi}{\partial\boldsymbol{\sigma}_\eta} = \left[-\frac{3\mu\left(\xi-\xi_{b1}\right)\left(\eta-\eta_{b1}\right)}{\rho_{13}^5} - \frac{3(1-\mu)\left(\xi-\xi_{b2}\right)\left(\eta-\eta_{b2}\right)}{\rho_{23}^5}\right]\left[\mathbf{h} - h_0 - (1+\lambda)h_0'\right] \tag{58}$$

$$\frac{\partial\mathcal{L}_\eta}{\partial\boldsymbol{\sigma}_\eta} = c^2\mathbf{h}'' + \left[-\frac{3\mu\left(\eta-\eta_{b1}\right)^2}{\rho_{13}^5} + \frac{\mu}{\rho_{13}^5} - \frac{3(1-\mu)\left(\eta-\eta b2\right)^2}{\rho_{23}^5} + \left[\frac{1-\mu}{\rho_{23}^5}\right]\right]\left[\mathbf{h} - h_0 - (1+\lambda)h_0'\right] \tag{59}$$

$$\frac{\partial\mathcal{L}_\eta}{\partial\boldsymbol{\sigma}_\xi} = \left[-\frac{3\mu\left(\xi-\xi_{b1}\right)\left(\eta-\eta_{b1}\right)}{\rho_{13}^5} - \frac{3(1-\mu)\left(\xi-\xi_{b2}\right)\left(\eta-\eta_{b2}\right)}{\rho_{23}^5}\right]\left[\mathbf{h} - h_0 - (1+\lambda)h_0'\right] \tag{60}$$

4.2. Solving the CR3BP boundary value problem, with equations in the inertial frame, via TFC

The boundary value problem can also be solved using TFC. In this case, it is sufficient to consider the boundary conditions in the matrix given in Eq. 11 instead of the initial conditions, as shown in Eq. 61.

$$\begin{bmatrix} \xi(\lambda_1) \\ \xi(\lambda_2) \\ \eta(\lambda_1) \\ \eta(\lambda_2) \end{bmatrix} = \begin{bmatrix} \mathbf{p}_\xi(\lambda_1) & \mathbf{q}_\xi(\lambda_1) & 0 & 0 \\ \mathbf{p}_\xi(\lambda_2) & \mathbf{q}_\xi(\lambda_2) & 0 & 0 \\ 0 & 0 & \mathbf{p}_\eta(\lambda_1) & \mathbf{q}_\eta(\lambda_1) \\ 0 & 0 & \mathbf{p}_\eta(\lambda_2) & \mathbf{q}_\eta(\lambda_2) \end{bmatrix}\begin{bmatrix} \nu_{1\xi} \\ \nu_{2\xi} \\ \nu_{1\eta} \\ \nu_{2\eta} \end{bmatrix} = \begin{bmatrix} \mathbf{g}(\lambda_1) \\ \mathbf{g}(\lambda_2) \\ \mathbf{g}(\lambda_1) \\ \mathbf{g}(\lambda_2) \end{bmatrix} \tag{61}$$

Following the same process, the following expressions can be obtained for the matrix Y and vector υ for the coordinates ξ (Eqs. 62 and 63) and η (Eqs. 64 and 65), respectively.

$$\mathrm{Y}_{\xi_{ij}} = c^2\mathbf{h}''(\lambda) + \mathbf{f}_{0\xi}(\lambda)\left[\mathbf{h}(\lambda) - \left(\frac{1-\lambda}{2}\right)h_0 - \left(\frac{1+\lambda}{2}\right)h_f\right] \tag{62}$$

$$\upsilon_{\xi_i}(\lambda) = f_\xi - f_{0\xi}\left[\left(\frac{\xi_0+\xi_f}{2}\right) + \left(\frac{\xi_f-\xi_0}{2}\right)\lambda\right] \tag{63}$$

$$\mathrm{Y}_{\eta_{ij}} = c^2\mathbf{h}''(\lambda) + \mathbf{f}_{0\eta}(\lambda)\left[\mathbf{h}(\lambda) - \left(\frac{1-\lambda}{2}\right)h_0 - \left(\frac{1+\lambda}{2}\right)h_f\right] \tag{64}$$

$$\upsilon_{\eta_i}(\lambda) = f_\eta - f_{0\eta}\left[\left(\frac{\eta_0+\eta_f}{2}\right) + \left(\frac{\eta_f-\eta_0}{2}\right)\lambda\right] \tag{65}$$

The constrained expressions become Eqs. 66 and 67,

$$\xi(\lambda) = \boldsymbol{\sigma}_\xi\left[\mathbf{h}(\lambda) - \left(\frac{1-\lambda}{2}\right)h_0 - \left(\frac{1+\lambda}{2}\right)h_f\right] + \left(\frac{\xi_0+\xi_f}{2}\right) + \left(\frac{\xi_f-\xi_0}{2}\right)\lambda \tag{66}$$

$$\eta(\lambda) = \boldsymbol{\sigma}_\eta\left[\mathbf{h}(\lambda) - \left(\frac{1-\lambda}{2}\right)h_0 - \left(\frac{1+\lambda}{2}\right)h_f\right] + \left(\frac{\eta_0+\eta_f}{2}\right) + \left(\frac{\eta_f-\eta_0}{2}\right)\lambda \tag{67}$$

where h_f is the function $\mathbf{h}(\lambda)$ calculated for $\lambda = 1$. The quantities ξ_0 and ξ_f are, respectively, the initial and final ξ positions, and η_0 and η_f are, respectively, the initial and final η positions.

Since the equation of motion is the same regardless of whether the problem is an IVP or a BVP, the loss function are the same (Eqs. 54 and 55) and, consequently, the Jacobian is also the same (Eqs. 57, 58, 59 and 60) for both problems.

4.3. Solving the CR3BP initial value problem, with equations in the rotating frame, via TFC

Let us now analyze the orbital dynamics in the rotating referential system. The equations of motion that describe the trajectory of body B_3 in this frame are given by Eqs. 68 and 69, where $\mathbf{r}_{13}$ and $\mathbf{r}_{23}$ are given by Eq. 70, for x and y, respectively (y and y are components of vector $\mathbf{r}_{23}$ illustrated in Figure 6).

$$\ddot{x} + \left[\frac{\mu}{|\mathbf{r}_{13}|^3} + \frac{(1-\mu)}{|\mathbf{r}_{23}|^3} - 1\right]x = 2\dot{y} + \frac{\mu(1-\mu)}{|\mathbf{r}_{13}|^3} - \frac{(1-\mu)\mu}{|\mathbf{r}_{23}|^3} \tag{68}$$

$$\ddot{y} + \left[\frac{\mu}{|\mathbf{r}_{13}|^3} + \frac{(1-\mu)}{|\mathbf{r}_{23}|^3} - 1\right]y = -2\dot{x} \tag{69}$$

$$\begin{aligned}\mathbf{r}_{13}^2 &= (x+\mu)^2 + y^2 + z^2 \\ \mathbf{r}_{23}^2 &= [x-(1-\mu)]^2 + y^2 + z^2\end{aligned} \tag{70}$$

These equations are already formatted as Eq. 1 and it is easy to identify the DE coefficients (Eqs. 71 and 72).

In Eqs. 68, 69 and 70, r_{13} is the distance from body B_1 (primary) to body B_3, r_{23} is the distance from body B_2 (secondary) to body B_3.

$$\begin{aligned}f_{2x} &= 1 \\ f_{1x} &= 0 \\ f_{0x} &= \frac{\mu}{|\mathbf{r}_{13}|^3} + \frac{(1-\mu)}{|\mathbf{r}_{23}|^3} - 1 \\ f_x &= 2\dot{y} + \frac{\mu(1-\mu)}{|\mathbf{r}_{13}|^3} - \frac{(1-\mu)\mu}{|\mathbf{r}_{23}|^3}\end{aligned} \tag{71}$$

$$\begin{aligned}f_{2y} &= 1 \\ f_{1y} &= 0 \\ f_{0y} &= \frac{\mu}{|\mathbf{r}_{13}|^3} + \frac{(1-\mu)}{|\mathbf{r}_{23}|^3} - 1 \\ f_y &= -2\dot{x}\end{aligned} \tag{72}$$

In Eqs. 71 and 72, f_{2x}, f_{1x}, f_{0x} and f_x are the equivalent values of $\mathbf{f}_2(t)$, $\mathbf{f}_1(t)$, $\mathbf{f}_0(t)$ and $\mathbf{f}(t)$, presented in Eq. 1, for Eq. 68 and f_{2y}, f_{1y}, f_{0y} and f_y are the equivalent values for Eq. 69.

In a rotating system, it is important to define the sphere of influence, which demarcates the limit at which the vehicle/satellite/body is considered captured or not.

The sphere of influence of the primary of radius r_E is given by 73.

$$\mathbf{r}_E = \left(\frac{\mu}{1-\mu}\right)^{\frac{2}{5}} \tag{73}$$

The following expressions can be obtained for the matrix Y and vector υ for the coordinates x (Eqs. 74 and 75) and y (Eqs. 76 and 77), respectively:

$$\mathrm{Y}_{x_{ij}} = c^2\mathbf{h}''(\lambda) + \mathbf{f}_{0x}(\lambda)\left[\mathbf{h}(\lambda) - h_0 - (1+\lambda)h_0'\right] \tag{74}$$

$$\upsilon_{x_i}(\lambda) = f_x - f_{0x}\left[x_0 + (1+\lambda)\frac{\dot{x}_0}{c}\right] \tag{75}$$

$$\mathrm{Y}_{y_{ij}} = c^2\mathbf{h}''(\lambda) + \mathbf{f}_{0y}(\lambda)\left[\mathbf{h}(\lambda) - h_0 - (1+\lambda)h_0'\right] \tag{76}$$

$$\upsilon_{y_i}(\lambda) = f_y - f_{0y}\left[y_0 + (1+\lambda)\frac{\dot{y}_0}{c}\right] \tag{77}$$

where $\mathrm{Y}_{x_{ij}}$ is the ij-th element of the matrix Y_x, which corresponds to the matrix Y used for the calculation of $x(\lambda)$, υ_{x_i} is the i-th element of the vector $\boldsymbol{\upsilon}_x$, which corresponds to the vector $\boldsymbol{\upsilon}$ used for the calculation of $x(\lambda)$ and $\mathrm{Y}_{y_{ij}}$ and $\boldsymbol{\upsilon}_{y_i}(\lambda)$ are the equivalent values for $y(\lambda)$.

The constrained expressions become Eqs. 78 and 79.

$$\mathbf{x}(\lambda) = \boldsymbol{\sigma}_x\left[\mathbf{h}(\lambda) - h_0 - (1+\lambda)h_0'\right] + \left(x_0 + \frac{\dot{x}_0}{c}\right) + \frac{\dot{x}_0}{c}\lambda \tag{78}$$

$$\mathbf{y}(\lambda) = \boldsymbol{\sigma}_y\left[\mathbf{h}(\lambda) - h_0 - (1+\lambda)h_0'\right] + \left(y_0 + \frac{\dot{y}_0}{c}\right) + \frac{\dot{y}_0}{c}\lambda \tag{79}$$

The loss functions for x and y are given by Eqs. 80 and 81 respectively, while the jacobian components are given by Eqs. 82, 83, 84 and 85.

$$\mathcal{L}_x(x,x'',y,y',\boldsymbol{\sigma}_x,\boldsymbol{\sigma}_y) = c^2x'' - 2cy' + \frac{\mu[x-x_{b1}]}{\left[(x-x_{b1})^2+(y-y_{b1})^2\right]^{3/2}} + \frac{(1-\mu)[x-x_{b2}]}{\left[(x-x_{b2})^2+(y-y_{b2})^2\right]^{3/2}} \tag{80}$$

$$\mathcal{L}_y(y,y'',x,x',\boldsymbol{\sigma}_y,\boldsymbol{\sigma}_x) = c^2y'' + 2cx' + \frac{\mu[y-y_{b1}]}{\left[(x-x_{b1})^2+(y-y_{b1})^2\right]^{3/2}} + \frac{(1-\mu)[y-y_{b2}]}{\left[(x-x_{b2})^2+(y-y_{b2})^2\right]^{3/2}} \tag{81}$$

$$\frac{\partial\mathcal{L}_x}{\partial\boldsymbol{\sigma}_x} = c^2\mathbf{h}'' + \left[-1 - \frac{3\mu(x-x_{b1})^2}{r_{13}^5} + \frac{\mu}{r_{13}^5} - \frac{3(1-\mu)(x-x_{b2})^2}{r_{23}^5} + \frac{1-\mu}{r_{23}^5}\right]\left[\mathbf{h} - h_0 - (1+\lambda)h_0'\right] \tag{82}$$

$$\frac{\partial\mathcal{L}_x}{\partial\boldsymbol{\sigma}_y} = \left[-\frac{3\mu(x-x_{b1})y}{r_{13}^5} - \frac{3(1-\mu)(x-x_{b2})y}{r_{23}^5}\right]\left[\mathbf{h} - h_0 - (1+\lambda)h_0'\right] - 2c\left[\mathbf{h}' - h_0'\right] \tag{83}$$

$$\frac{\partial\mathcal{L}_y}{\partial\boldsymbol{\sigma}_y} = c^2\mathbf{h}'' + \left[-1 - \frac{3\mu y^2}{r_{13}^5} + \frac{\mu}{r_{13}^5} - \frac{3(1-\mu)y^2}{r_{23}^5} + \frac{1-\mu}{r_{23}^5}\right]\left[\mathbf{h} - h_0 - (1+\lambda)h_0'\right] \tag{84}$$

$$\frac{\partial\mathcal{L}_y}{\partial\boldsymbol{\sigma}_x} = \left[-\frac{3\mu(x-x_{b1})y}{r_{13}^5} - \frac{3(1-\mu)(x-x_{b2})y}{r_{23}^5}\right]\left[\mathbf{h} - h_0 - (1+\lambda)h_0'\right] + 2c\left[\mathbf{h}' - h_0'\right] \tag{85}$$

where x_{b1} and y_{b1} are the equivalent components x and y for the body B_1, x_{b2}, and y_{b2} are the equivalent components x and y for the body B_2, and $\mathcal{L}_x$ and $\mathcal{L}_y$ are the loss function for each component individually.

4.4. Solving the CR3BP boundary value problem, with equations in the rotating frame, via TFC

The boundary value problem for the equations in the rotating frame is presented next: the following expressions can be obtained for the matrix Y and vector υ for the coordinates x (Eqs. 86 and 87) and y (Eqs. 88 and 89), respectively:

$$\mathrm{Y}_{x_{ij}} = c^2\mathbf{h}''(\lambda) + \mathbf{f}_{0x}(\lambda)\left[\mathbf{h}(\lambda) - \left(\frac{1-\lambda}{2}\right)h_0 - \left(\frac{1+\lambda}{2}\right)h_f\right], \quad (86)$$

$$\upsilon_{x_i}(\lambda) = f_x - f_{0x}\left[\left(\frac{x_0+x_f}{2}\right) + \left(\frac{x_f-x_0}{2}\right)\lambda\right], \quad (87)$$

$$\mathrm{Y}_{y_{ij}} = c^2\mathbf{h}''(\lambda) + \mathbf{f}_{0y}(\lambda)\left[\mathbf{h}(\lambda) - \left(\frac{1-\lambda}{2}\right)h_0 - \left(\frac{1+\lambda}{2}\right)h_f\right], \quad (88)$$

$$\upsilon_{y_i}(\lambda) = f_y - f_{0y}\left[\left(\frac{y_0+y_f}{2}\right) + \left(\frac{y_f-y_0}{2}\right)\lambda\right]. \quad (89)$$

The constrained expressions become Eqs. 90 and 91:

$$\mathbf{x}(\lambda) = \boldsymbol{\sigma}_x\left[\mathbf{h}(\lambda) - \left(\frac{1-\lambda}{2}\right)h_0 - \left(\frac{1+\lambda}{2}\right)h_f\right] + \left(\frac{x_0+x_f}{2}\right) + \left(\frac{x_f-x_0}{2}\right)\lambda, \quad (90)$$

$$\mathbf{y}(\lambda) = \boldsymbol{\sigma}_y\left[\mathbf{h}(\lambda) - \left(\frac{1-\lambda}{2}\right)h_0 - \left(\frac{1+\lambda}{2}\right)h_f\right] + \left(\frac{y_0+y_f}{2}\right) + \left(\frac{y_f-y_0}{2}\right)\lambda. \quad (91)$$

The same comment regarding the loss functions and the Jacobian is valid here. The expressions are the same, regardless of whether the problem is an IVP or a BVP.

5. TEMPORARY GRAVITATIONAL CAPTURE VIA THEORY OF FUNCTIONAL CONNECTIONS

Temporary gravitational capture is defined by Yamakawa (1992) and Prado & Vieira Neto (2006) as a process in which a particle approaching from outside the sphere of influence may attain a low relative velocity with a celestial body and even rotate around it temporarily without utilizing any other effects than the gravitational force.

In many cases, the system is composed of three bodies, in which one body (B_3) orbits a primary and is subject to disturbance from the third body (B_2). Therefore, this case can be modeled through the restricted three-body problem in either its circular or elliptical version. In this study, only the circular version is addressed.

The B_3 trajectory is simulated (usually using numerical integration) in the backward time direction. Every escape in backward time (this means crossing the sphere of influence $\mathbf{r}_E$) corresponds to a gravitational capture in the forward time (Earth-moon, 2006).

By analyzing the equations of Y matrix and υ vector for the cases presented previously, it can be observed that it is necessary to know the values of ρ_{13} and ρ_{23} (considering the equations in the inertial system) or r_{13} and r_{23} (considering the equations in the rotating system) for each value of λ_i to perform the calculations. Therefore, it is necessary to start the method with these approximate values. For example, numerical integration can be performed using a simple integrator.

Let's take, as an example, an orbit analyzed in Yamakawa's thesis (Yamakawa, 1992) (page 45, orbit 2). This is the Earth-Moon-Sun system, where the movement of the Moon around the Earth is studied, with the perturbation by the Sun. The trajectories in the inertial frame and in the rotating frame are illustrated in Figures 7 and 8. These results were generated from a numerical integration through the initial conditions provided in Yamakawa's thesis, considering the CR3BP.

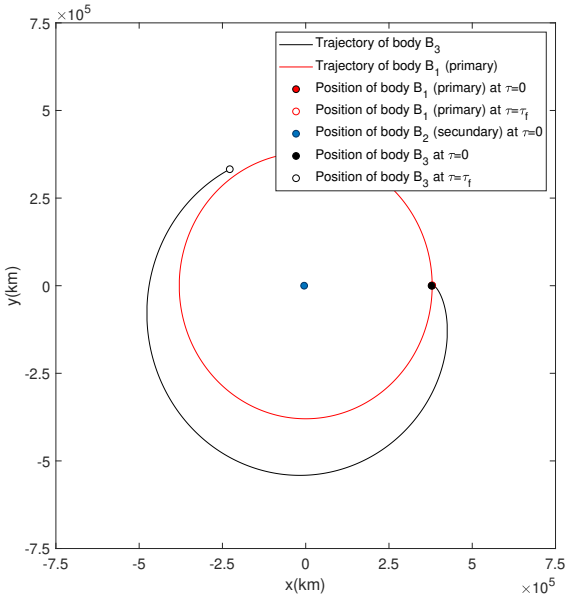

Figure 7. Moon's orbit in the Earth-Moon-Sun system presented in the inertial frame. Reproduction of orbit 2, on page 45, from Hiroshi Yamakawa's doctoral thesis.

Table 1. Organization of Subfigure Indices for Figures 9 and 10

Figure	Axis	IVP/BVP	Frame
9(a) and 10(a)	ξ	IVP	Inertial
9(b) and 10(b)	η	IVP	Inertial
9(c) and 10(c)	x	IVP	Rotating
9(d) and 10(d)	y	IVP	Rotating
9(e) and 10(e)	ξ	BVP	Inertial
9(f) and 10(f)	η	BVP	Inertial
9(g) and 10(g)	x	BVP	Rotating
9(h) and 10(h)	y	BVP	Rotating

The range of interest here is within the borders of the Earth's sphere of influence (body B_1). This same trajectory was calculated via TFC for each of the previously presented forms (IVP-inertial, BVP-inertial, IVP-rotating, IVP-rotating). For each of these cases, the error was evaluated versus the number of terms of the polynomial series (m) (Figure 9) and the number of time instants evaluated (N) (Figure 10).

The errors (ϵ) are presented in Figures 9 and 10 as a function of m and N, respectively. The errors are presented in $log_{10}\epsilon$ form to facilitate their visualization. The subfigure indices in Figures 9 and 10 are organized according to the layout presented in Table 1.

For each case presented in Figure 9 the error was evaluated in a range of m from 5 to 25 terms of polynomial series and N from m to $4 \times m$. For example, for $m = 5$, the range of N is from 5 to 20; for $m = 6$, the range of N is from 6 to 24; etc. The error reduces slightly for all cases except $N = 20$, which presents a decreasing curve versus m with a significant reduction near $m = 20$. This is because when the matrix Y is almost square, the errors are smaller, and when $m = N$ they are minimal for the calculation of

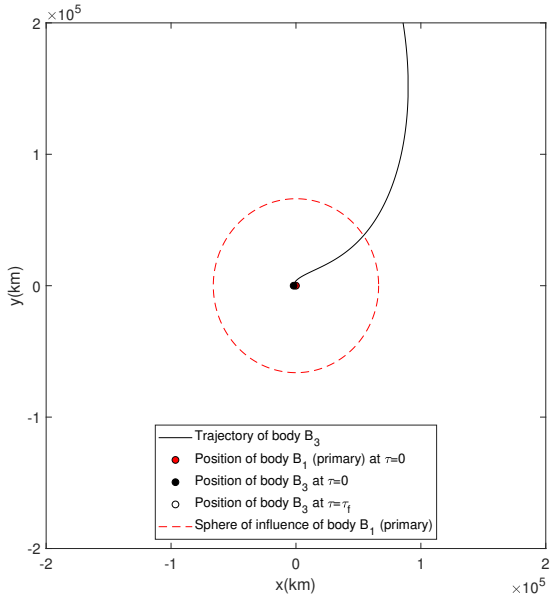

Figure 8. Moon's orbit in the Earth-Moon-Sun system presented in the rotating frame. Reproduction of orbit 2, on page 45, from Hiroshi Yamakawa's doctoral thesis.

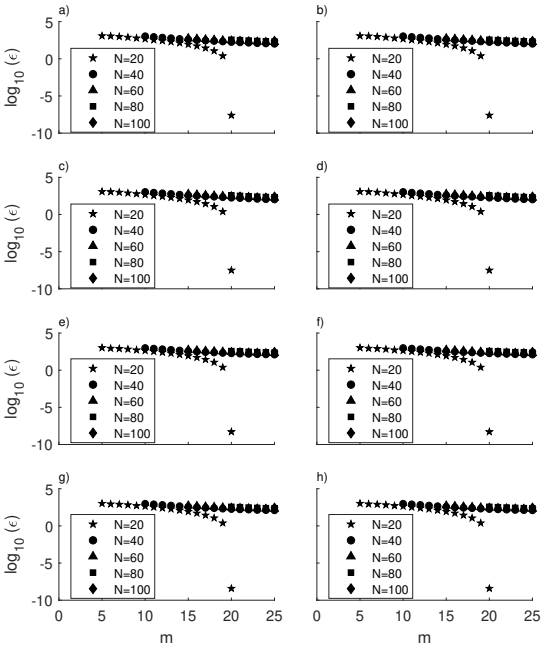

Figure 9. Log base 10 of error (ϵ) in function of the number of polynomials for Moon's orbit in the Earth-Moon-Sun system (case for Yamakawa's doctoral thesis). Initial value problem cases: (a)(b)(c)(d). Boundary value problem cases: (e)(f)(g)(h). Inertial system: (a)(b)(e)(f). Rotating system: (c)(d)(g)(h). x or ξ axis: (a)(c)(e)(g). y or η axis: (b)(d)(f)(h).

σ_0. The system is determined for $m = N$ and the solution is given directly by the inversion of the matrix Y. In cases where $N > m$, the solution is approximately given by the least-squares method.

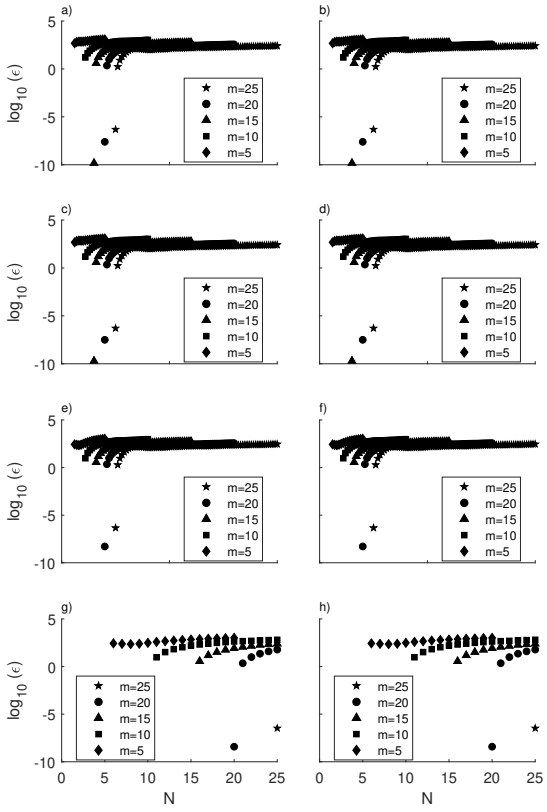

Figure 10. Log base 10 of error (ϵ) in function of the number of instant of times (N) in that the solution is evaluated for Moon's orbit in the Earth-Moon-Sun system (case for Yamakawa's doctoral thesis). Initial value problem cases: (a)(b)(c)(d). Boundary value problem cases: (e)(f)(g)(h). Inertial system: (a)(b)(e)(f). Rotating system: (c)(d)(g)(h). x or ξ axis: (a)(c)(e)(g). y or η axis: (b)(d)(f)(h).

Another behavior observed in Figure 9 is that as the number of terms in the Legendre polynomial series increases, the error (ϵ) decreases (albeit discreetly), because the series represents the solution more accurately.

Another notable fact is that the behavior of all curves (different values of N) is very similar between all sub-Figures (a), (b), (c), (d), (e), (f), (g), and (h), being therefore indifferent to the type of system chosen (inertial or rotating) and to the type of problem for solving the differential equations (IVP or BVP). A comparison between these errors is presented later in this paper.

For each case presented in Figure 10 the error was evaluated under the same conditions as in the previous case (Figure 9).

The error increases slightly for all cases and presents a significant reduction for low values of N. This reduction, as in the case of Figure 9, always occurs for cases where the value of N approaches the value of m, and is minimum for $m = N$. This is also because when the matrix Y is almost square, the errors are smaller, and when $m = N$ they are minimal for the calculation of σ_0.

Another behavior observed in Figure 10 is that in the regions where N is sufficiently greater than m, which means the "flat" error zone, as the number of points evaluated (N) increases, the error increases slightly. This occurs because there is a loss of

Table 2. Organization of Subfigure Indices for Figures 11 and 12

Figure	Data
Figures 11(a) and 12(a)	Ratio between the error (ϵ) for calculation of ξ-axis from the orbit calculated through the IVP in the Inertial System, and the error (ϵ) for calculation of x-axis from the orbit calculated through the IVP in the Rotating System.
Figures 11(b) and 12(b)	Ratio between the error (ϵ) for calculation of η-axis from the orbit calculated through the IVP in the Inertial System, and the error (ϵ) for calculation of y-axis from the orbit calculated through the IVP in the Rotating System.
Figures 11(c) and 12(c)	Ratio between the error (ϵ) for calculation of ξ-axis from the orbit calculated through the BVP in the Inertial System, and the error (ϵ) for calculation of x-axis from the orbit calculated through the IVP, in the Rotating System.
Figures 11(d) and 12(d)	Ratio between the error (ϵ) for calculation of η-axis from the orbit calculated through the BVP in the Inertial System, and the error (ϵ) for calculation of y-axis from the orbit calculated through the IVP in the Rotating System.
Figures 11(e) and 12(e)	Ratio between the error (ϵ) for the calculation of x-axis from the orbit calculated through the BVP in the Rotating System, and the error (ϵ) for the calculation of x-axis from the orbit calculated through the IVP in the Rotating System.
Figures 11(f) and 12(f)	Ratio between the error (ϵ) for the calculation of y-axis from the orbit calculated through the BVP, in the Rotating System and the error (ϵ) for the calculation of y-axis from the orbit calculated through the IVP, in the Rotating System.

response quality via TFC when evaluating the solution at more points. The greater the number of time instants to be evaluated, the greater the number of terms in the polynomial series needed to keep the errors at a satisfactory level; otherwise, the matrix $\mathrm{Y}_{N\times m}$ begins to present $N >> m$ and deliver a not very accurate solution.

As shown in Figure 9 the behavior shown in all subfigures of Figure 10 is very similar, aside from the type of system chosen (inertial or rotating) and to the type of problem for solving the differential equations (IVP or BVP).

All these cases presented an initial solution error $\boldsymbol{\sigma}_0$. However, with some iterations (in the order of 2 to 5), it is possible to obtain an error of less than 10^{-12} using the linearization of the DE around the initial solution, as presented previously.

We now compare the errors for different frames and numerical integration problems. In celestial mechanics studies, the most common case is the IVP in the rotating frame because it is easy to specify the initial conditions in this frame, and in general, the aim is to make the trajectory of the body as a function of time, without necessarily a spatial constraint at another instant in time, except in studies such as orbital transfers. Therefore, this case will be considered as the reference, and the errors of each of the other cases will be compared with this one.

The same case studied in Figures 7, 8, 9 and 10 is simulated in a range of m between 5 and 25 and N between m and $4 \times m$ is used to present the ratio between errors using different coordinate systems and the numerical integration problem. The comparisons are illustrated in Figures 11 and 12. The subfigure indices in Figures 11 and 12, which present the dimensionless values (ϵ/ϵ), are organized according to the layout presented in Table 2.

Figure 11 presents the error ratio as a function of the number of polynomials considered in the series (m) and the number of instants at which the solution is evaluated (N). This shows that the regions close to $m = N$ present a significant variation in errors depending on the method chosen for the simulation. This is due to the shape of the trajectories, which ends up altering the matrix Y and consequently the quality of the solution of the system given by Eq. 22. This effect can be easily observed in the change in the shape of the trajectories in the TFC method by analyzing Figures. 7 and 8 as an example and observing Eqs. 48, 49, 50, 51, 62, 63, 64, 65, 74, 75, 76, 77, 86, 87, 88 and 89. For regions not close to $m = N$ the difference between the errors is significantly small, which is demonstrated by an error ratio close to 1.

Figure 12 shows that for a m greater than 10 and $N > m$, the errors between the different strategies are equivalent. Very small values of m are not practical and useful because, in those cases, even using DE linearization, it is not possible to reduce the value of errors at the machine level. In these cases, it is necessary to increase the number of polynomials until the desired level of accuracy is achieved.

Figure 12 also shows that for $N = m$ there is an error oscillation when we compare the inertial and rotating frame data. It is also possible to conclude for the BVP cases (c),(d),(e), and (f) that the errors of the TFC calculation for the BVP problem are higher than the errors for the same TFC calculation with the IVP problem (in the rotating frame) for $m > 15$, which in practical terms suggests that calculation through a BVP may not be the best option, or at least not the most optimized one.

These local conclusions should be considered quite restricted, since they refer to only one well-defined trajectory (the case cited above in Dr. Yamakawa's thesis), and there is the possibility that they are not universal.

Future studies should investigate whether this behavior can be verified independently of the studied system and initial conditions (or contour conditions). Currently, it is worth noting that the errors are equivalent and that each case may be interesting for a particular type of study. IVPs may be useful for studying the temporal response of a system, including cases in which perturbations occur with non-conservative forces. BVPs are useful for studying orbital transfer and gravitational capture cases, where the starting and end points in the sphere of influence of the primary are specified.

It is also worth noting that this study aims to compare the different ways of using the TFC method, focusing especially on

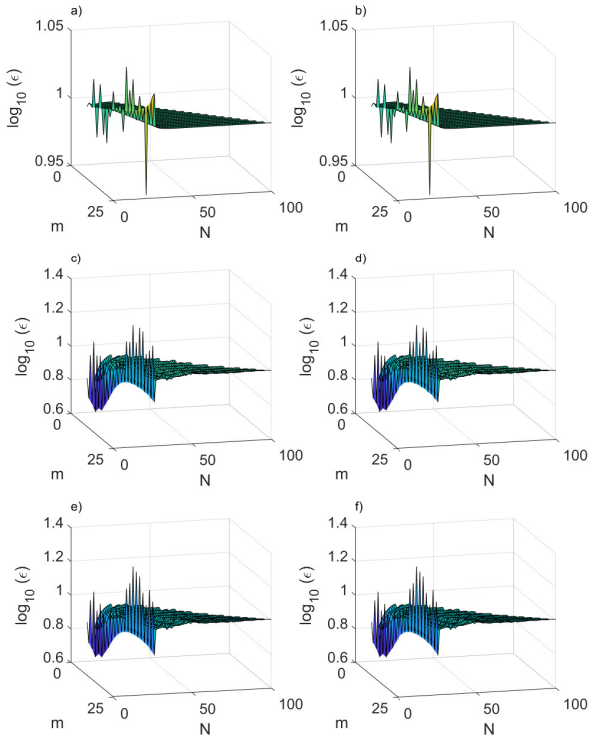

Figure 11. Ratio between errors of IVP in Inertial frame (a) and (b), BVP in Inertial frame (c) and (d), BVP in Rotating frame (e) and (f) and the reference IVP in Rotating frame in function of number of terms of polynomial series considered in the calculations. See Table 2 for caption details.

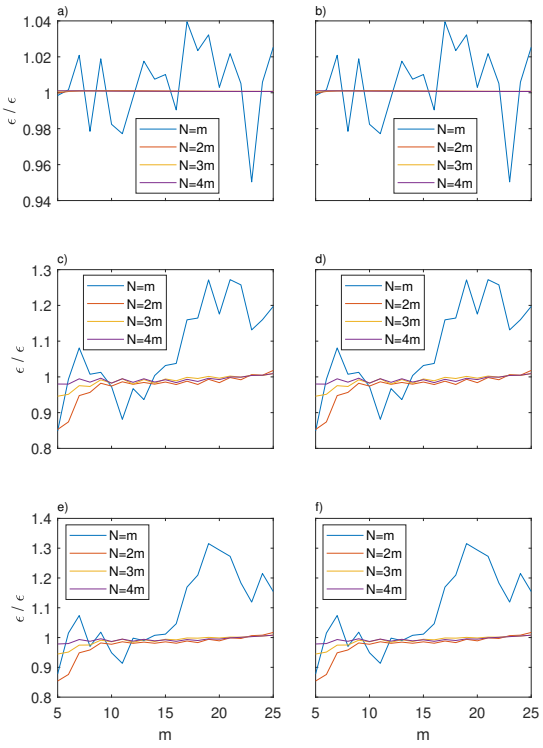

Figure 12. Ratio between errors of (IVP - Inertial) or (BVP - Inertial) or (BVP - Rotating frame) and the reference (IVP-Rotating frame) in function of total instant of times evaluated. See Table 2 for caption details.

the initial solution ($\boldsymbol{\sigma}_0$). The TFC method allows, as already stated above, to obtain a solution with machine error level error with few iterations.

Finally, we will reflect on the conditions in which there is capture (escape in backward integration) or not captured (collision with the primary or orbit without crossing the sphere of influence). The solution of system given by Eq. 22 depends on the reversal of the matrix Y, whether it is a direct inverse through a method such as Moore-Penrose or through a pseudo-inverse as in methods QR decomposition, SVD decomposition and Cholesky decomposition (Leake et al., 2022).

Suppose we want to study a boundary value problem in a rotating system. If the initialization of the method (values of $\mathbf{r}_{13}$ and $\mathbf{r}_{23}$) is performed arbitrarily and intuitively, without the use of numerical integration, it should be impossible to solve the system because Y should not present an inverse, or if an initial solution is obtained, the solution certainly should diverge in the "optimization" step because the solution cannot converge to the final solution. Future studies may address these verifications, including the application of the expressions derived in this study.

6. CONCLUSIONS

The problem of gravitational capture, modeled through the circular restricted problem of three bodies, can be solved through the TFC, both for the initial value and boundary value problems in both reference systems (inertial or rotating).

The initial TFC solution (before optimization) has a lower error when the number of polynomials used in the calculation is equal to the total number of time instants evaluated. This is due to the fact that the matrix Y is square.

For the case analyzed in this study, from the Yamakawa thesis, errors for the initial solution ($\boldsymbol{\sigma}_0$) were equivalent for all cases except for the IVP in the rotating system, which presented a lesser response to $m > 10$.

The inverse of the matrix Y is a means to infer whether gravitational capture is possible in a time interval [0 -t_f], as it indicates whether there is an exhaust from the influence sphere in a backward integration.

The author expresses sincere gratitude to Dr. Daniele Mortari for the development of the Theory of Functional Connections.

Financial support was provided by the National Council for Scientific and Technological Development (CNPq), project 309089/2021-2.

REFERENCES

Belbruno, E. 1987, Lunar capture orbits, a method of constructing earth moon trajectories and the lunar GAS mission, doi: 10.2514/6.1987-1054

Belbruno, E. 2004, Capture Dynamics and Chaotic Motions in Celestial Mechanics: With Applications to the Construction of Low Energy Transfers, (Princeton, NJ: PUP), 232

Belbruno, E., Gidea, M., & Topputo, F. 2010, SIAM Journal on Applied Dynamical Systems, 9, 1061, doi: 10.1137/090780638

Belbruno, E., Topputo, F., & Gidea, M. 2008, AdSpR, 42, 1330, doi: 10.1016/j.asr.2008.01.018
Belbruno, E. A., & Miller, J. K. 1993, JGCD, 16, 770, doi: 10.2514/3.21079
Circi, C., & Teofilatto, P. 2001, CeMDA, 79, 41, doi: 10.1023/A:1011153610564
Dahlke, S. R. 1998, Investigation of lunar ballistic capture transfer trajectories, PhD thesis, University of Colorado at Boulder
de Almeida Junior, A. K., Johnston, H., Leake, C., & Mortari, D. 2021, EPJP, 136, 223, doi: https://doi.org/10.1140/epjp/s13360-021-01151-2
Earth-moon, T. 2006, Journal of the Brazilian Society of Mechanical Sciences and Engineering, XXVIII, 347, doi: 10.1590/S1678-58782006000300013
García, F., & Gómez, G. 2007, CeMDA, 97, 87, doi: 10.1007/s10569-006-9053-6
Johnston, H., Leake, C., & Mortari, D. 2020, Mathematics, 8, 397, doi: 10.3390/math8030397
Lanczos, C. 1957, Applied Analysis (New York, NY, USA: Dover Publications Inc.), 504
Leake, C., Johnston, H., & Mortari, D. 2022, The Theory of Functional Connections: A Functional Interpolation Framework with Applications, 1st edn. (Lulu.com), 160
Li, J., & Sun, Y. S. 2015, RAA, 15, 376, doi: 10.1088/1674-4527/15/3/007
Machuy, A. L., Prado, A. F. B. A., & Stuchi, T. J. 2007, AdSpR, 40, 118, doi: 10.1016/j.asr.2007.02.069
Mortari, D. 2017a, Mathematics, 5, 48, doi: 10.3390/math5040048
—. 2017b, Mathematics, 5, 57, doi: 10.3390/math5040057
Mortari, D., Johnston, H., & Smith, L. 2019, JCoAM, 352, 293, doi: 10.1016/j.cam.2018.12.007
Neto, E. V., & de Almeida Prado, A. F. B. 1998, JGCD, 21, 122, doi: 10.2514/2.4207
Prado, A. F. B. d. A., & Vieira Neto, E. 2006, JAnSc, 54, 567, doi: 10.1007/BF03256506
Topputo, F., & Belbruno, E. 2009, CeMDA, 105, 3, doi: 10.1007/s10569-009-9222-5
—. 2015, CeMDA, 121, 329, doi: 10.1007/s10569-015-9605-8
Wright, K. 1964, Computer Journal, 6, 358
Yamakawa, H. 1992, PhD thesis, University of Tokyo, doi: 10.11501/3095448
Yamakawa, H., Kawaguchi, J., Ishii, N., & Matsuo, H. 1992, in Spaceflight Mechanics 1992, ed. R. E. Diehl, R. G. Schinnerer, W. E. Williamson, & D. G. Boden, 1113–1132, doi: 1992sfm..proc.1113Y
Yamakawa, H., Kawaguchi, J. I., Ishii, N., & Matsuo, H. 1993, in Proceedings of the AAS/AIAA Astrodynamics Conference. Part 3 (of 3) (Univelt Inc.), 397
Yamakawa, H., & Yawaguchi, A. 1993, in IEEJ Trasactions on Electronics, Information and Systems, Vol. 113, 621, doi: 10.1541/ieejeiss1987.113.8_621